J Mater Sci (2009) 44:6701–6709
DOI 10.1007/s10853-009-3602-9

MESOSTRUCTURED MATERIALS

Pt nanoparticles inside the mesopores of TiO_2–MCM-48: synthesis, characterization and catalytic activity for CO oxidation

Vaishali V. Narkhede · Andrea De Toni · Vijay S. Narkhede · Markus Reichinger · A. Birkner · J. W. (Hans) Niemantsverdriet · Wolfgang Grünert · Hermann Gies

Received: 10 November 2008 / Accepted: 14 May 2009 / Published online: 18 June 2009

Abstract TiO_2 and Pt nanoparticles were deposited in the channels of siliceous MCM-48 via a sequential incipient wetness-impregnation method employing $(NH_4)_2PtCl_4$ as platinum source. The resulting composite Pt/TiO_2–MCM-48 (1 wt% Pt, ca. 3 wt% Ti) was characterized using XRD, TEM, nitrogen physisorption, hydrogen chemisorption, UV–vis spectroscopy, and XPS; its catalytic activity for CO oxidation was also explored. These data were compared with those of Pt/MCM-48 prepared via an analogous route. The results reveal that the platinum was deposited inside the intact pore system in both cases. It remains inside upon mild reduction but tends to segregate out of the pore system at higher reduction temperatures or during CO oxidation. Both composites were found to be highly active in CO oxidation, with 50% conversion at 460–475 K after activation of the unreduced catalysts in the (net oxidizing) feed. Striking differences in this activation process between Pt/MCM-48 and Pt/TiO_2–MCM-48 suggest that the precursor reduction is influenced by an interaction with the TiO_2 component in the latter.

V. V. Narkhede · M. Reichinger · H. Gies (✉)
Chair of Crystallography, Institute of Geology, Mineralogy and Geophysics, Ruhr-University Bochum, 44780 Bochum, Germany
e-mail: hermann.gies@rub.de

A. De Toni · W. Grünert (✉)
Laboratory of Industrial Chemistry, Faculty of Chemistry and Biochemistry, Ruhr-University Bochum, 44780 Bochum, Germany
e-mail: w.gruenert@techem.rub.de

V. S. Narkhede · J. W. Niemantsverdriet
Schuit Institute of Catalysis, Eindhoven University of Technology, 5600 MB Eindhoven, The Netherlands

A. Birkner
Laboratory of Physical Chemistry I, Faculty of Chemistry and Biochemistry, Ruhr-University Bochum, 44780 Bochum, Germany

Introduction

Since the discovery of novel class of mesoporous M41S materials by Mobil researchers [1, 2], much application-oriented research has been performed in order to find innovative uses for these new materials. Because of their pore size in the range between 2 and 10 nm, their narrow pore-size distributions, and composition related to zeolites, most inspiration for research activities came from the zeolite community. The composition of the M41S family of materials is restricted to silicate frameworks; MCM-41 (with hexagonal honeycomb symmetry), MCM-48 (with cubic *Ia*3*d* symmetry) and MCM-50 (a lamellar phase) are the three mesoporous silicate host structures of this family. The properties of these materials were explored for sorption, separation, and catalytic processes. Relevant review articles on these activities are available in the literature [3, 4].

Another area of application-oriented interest for the silica-based materials such as MCM-41/48, SBA-15, etc., could be their use as carriers or matrices for functional molecules or nanoparticles [5–7]. Because of their high thermal and chemical stability, and their mechanical robustness the silica-based mesoporous materials have attracted much attention. Their mesoporous structures can thus be explored as host or matrix to immobilize catalytically active species and, simultaneously, for providing nano-size confinement inside the channel system. Literature is available on highly dispersed metal or metal oxide nanoparticles inside the one-dimensional pore system of

SBA-15 and MCM-41 materials [8]; however, despite the advantage of a 3d pore system, such studies on MCM-48 materials with 3d channel system are scarce, probably due to the difficulty in the preparation of MCM-48 in suitable quality. Recently, we reported on the deposition of Cu, Zn acetates within the pore system of mesoporous MCM-48 and their subsequent decomposition to metal oxide nanoclusters [9, 10]. Furthermore, we also explored and analyzed the deposition of TiO_2 particles into MCM-48 as a support for size-confined Au particles [11–13]. Subsequent deposition of gold nanoparticles into this TiO_2-containing MCM-48 resulted in a catalyst, highly active in CO oxidation [12, 13]. Such catalysts can be useful for mechanistic studies on the role of the support in the catalytic process because of the dispersion of the active component in the 3d channel system and because the quantities of support (ZnO, TiO_2) and metal (Cu, Au) are in the same order of magnitude.

To the best of our knowledge, no reports regarding the impregnation of Pt inside the pore system of TiO_2–MCM-48 have been published to date. Pt/TiO_2 is one of the classical systems in which strong metal–support interaction (SMSI) can be observed [14]. There are few reports on the direct deposition of Pt in MCM-41/48 without TiO_2 [15, 16]. Here, we report a successful synthesis of Pt/TiO_2–MCM-48 material using incipient wetness-impregnation method. The composites underwent thorough characterization by means of X-ray powder diffraction (XRD), Transmission Electron Microscopy (TEM), Inductively Coupled Plasma-Atomic Emission Spectroscopy (ICP-AES), porosity analysis by nitrogen physisorption, H_2-chemisorption, diffuse reflectance UV–visible spectroscopy (UV–vis), and X-ray photoelectron spectroscopy (XPS). We also report on first results of CO oxidation as catalytic test reaction.

Experimental

Synthesis

The basic method for preparation of highly dispersed platinum nanoparticles in the pores of cubic MCM-48 is straightforward and exemplified in Fig. 1.

The preparation of pure mesoporous silica MCM-48 was carried out according to the method described by Gies et al. [9]. The final molar gel composition of the synthesis mixture was 1 (TEOS):0.70 (CTACl):0.5 (NaOH):64 (H_2O). This mixture was stirred at 323 K for 15 min and then transferred to an oven heated at 363 K for 4 days. The resulting solid was filtered, thoroughly washed with distilled water, dried overnight at room temperature, and calcined at 813 K for 5 h at a heating rate of

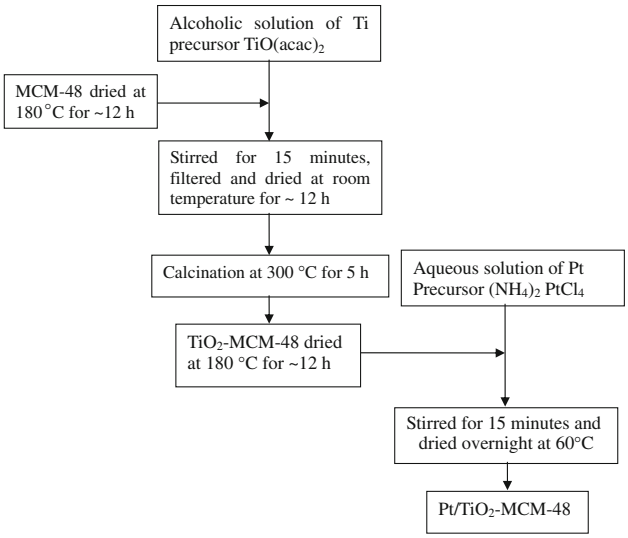

Fig. 1 Schematic representation of the preparation of Pt/TiO_2–MCM-48 catalyst using incipient wetness-impregnation method

1 K/min. TiO_2–MCM-48 was prepared via a post-synthetic wet-impregnation method using titanylacetylacetonate ($TiO(acac)_2$, Merck) as a titanium precursor [11]. In short, an appropriate amount of $TiO(acac)_2$ was dissolved in the equivalent ratio of ethanol–water mixture which gives a clear solution of $TiO(acac)_2$. During the impregnation, calcined MCM-48 was added to the alcoholic solution of $TiO(acac)_2$ with vigorous stirring for 15 min. The resulting mixture was filtered and washed thoroughly with distilled water, and dried at room temperature overnight. Thereafter, the thermal decomposition of the metal acetylacetonate was performed in a muffle oven in air by heating the sample at 573 K for 5 h after ramping the temperature at 1 K/min.

Pt was introduced into TiO_2–MCM-48 or bare MCM-48 utilizing an incipient wetness-impregnation method in which the aqueous Pt precursor solution ($(NH_4)_2PtCl_4$, Sigma–Aldrich, 1.78×10^{-2} M) was stirred with the mesoporous support. The resulting composite was initially dried at room temperature overnight, subsequent to drying at 333 K for 12 h. The composition of the samples as determined by ICP–AAS is reported in Table 1.

Characterization of the synthesis products

The degree of crystallinity and morphology of the obtained Pt/TiO_2–MCM-48 material was studied using X-ray diffraction (XRD) and transmission electron microscopy (TEM). X-ray powder diffraction experiments were carried out using a Huber Guinier imaging plate camera G670 with Cu $K\alpha_1$ radiation ($\lambda = 1.5418$ Å) by loading the sample into a glass capillary. A Siemens D5000 diffractometer with Cu $K\alpha_1$ radiation in modified Debye Scherrer

Table 1 Nitrogen sorption and elemental analysis results of MCM-48, TiO_2–MCM-48, and Pt/TiO_2–MCM-48

Sample	BET surface area (m^2/g)	BJH pore volume (cm^3/g)	Average pore diameter (Å)	Elemental analysis by ICP-AES (wt%)
MCM-48	1184	0.87	24.8	–
TiO_2–MCM-48	1094	0.74	23.0	2.87 (Ti)
Pt/TiO_2–MCM-48	1008	0.68	22.4	1.0 (Pt)
Pt/MCM-48	980	0.80	25	1.75 (Pt)

geometry was employed for low angle XRD measurements. Transmission electron microscopy (TEM) was performed using a Hitachi H-8100 instrument operating at 200 kV. The elemental chemical analysis of the composite was carried out using ICP–AES using a UNICAM PU 7000 instrument.

The surface area and pore parameters of the samples were analyzed by nitrogen adsorption–desorption measurements at 77 K on Micromeritics Tristar 3000. Prior to the experiments, the samples were outgassed at 373 and 423 K, holding each temperature for 3 h, under vacuum in a degassing port of the adsorption analyzer. The BET surface area was determined by multipoint BET method using adsorption data in the relative pressure (p/p_0) range of 0.06–0.20. The desorption branch of the nitrogen isotherm was used to determine the mesopore-size distribution using the Barret, Joyner, and Halenda (BJH) method and the average pore sizes were obtained from the peak position of the distribution curves. In order to be able to compare results obtained for the different samples, surface areas and pore volumes are scaled to the same amount of siliceous MCM-48.

UV–vis diffuse reflectance spectra measurements were carried out using a Shimadzu UV 2401 instrument in the range of 200–800 nm. X-ray photoelectron spectra (XPS) were recorded using a Kratos Axis Ultra DLD spectrometer equipped with a standard Al Kα excitation source ($h\nu = 1486.6$ eV) and hemispherical analyzer operated at a constant pass energy of 40 eV. The appropriate corrections for the charging effect were made with help of the Si 2p signal, which was set at 103.4 eV. The hydrogen chemisorption capacity was determined volumetrically with an Autosorb 1C setup (Quantachrome). The chemisorption capacity was first determined after reduction in pure hydrogen at 573 K and subsequently after reduction at 773 K. With Pt/TiO_2–MCM-48, the sample was then re-oxidized in oxygen at 773 K and re-reduced at 573 K to perform a final chemisorption measurement because SMSI is known to be a reversible phenomenon.

CO oxidation was performed at atmospheric pressure and at temperatures in the range of 300–570 K, using a glass-lined U-tube, plug flow reactor with an inner diameter of 4 mm. The measurements were conducted both under dynamic conditions while ramping the temperature with 2 K/min and under stationary conditions (cf. Fig. 9). The reaction temperature was measured directly in the fixed bed using a K-type thermocouple. A mixture of 1% CO in synthetic air (pre mixed) was passed over 50 mg of catalyst (grain size 250–500 μm) with a flow rate of 67 mL/min, which corresponds to a space velocity of 80,000 mL h^{-1} g_{cat}^{-1}. In the first run, the catalyst was used in the "as-synthesized" state, i.e., it was not reduced before exposure to the feed. Consecutive temperature cycles were performed to explore the catalyst stability during reaction. Both CO and CO_2 concentrations were measured using an Uras 26 infrared analyzer module (ABB Corp.). The analytical scheme was backed up with a Pfeiffer Omnistar quadrupole mass spectrometer for qualitative detection of components from precursor decomposition.

Results and discussion

The small angle X-ray diffraction patterns of pristine MCM-48, TiO_2–MCM-48, and the Pt-loaded matrices are shown in Fig. 2a. The low-angle diffractogram of pure siliceous MCM-48 clearly shows that the MCM-48 material, synthesized using the conventional hydrothermal procedure possessed excellent periodicity. According to the XRD pattern of MCM-48, an intense reflection peak at $2\theta = 2.56°$ (d_{211}) together with a weak shoulder reflection peak at $2\theta = 2.98°$ (d_{220}) clearly reveals the characteristics of the cubic structure of MCM-48 (space group symmetry *Ia3d*). Deposition of platinum or of TiO_2 inside the pore system of TiO_2–MCM-48 both leads to a decrease of XRD peak intensities. However, the crystallinity of siliceous MCM-48 remains unchanged, as can be seen in the X-ray diffractograms of the composites which show unchanged peak widths. The remarkable decrease of the peak intensity is due to the fact that pore filling reduces the scattering contrast between pores and pore walls of MCM-48 typical for non-crystalline mesoporous materials [9]. Deposition of platinum inside the pore system of TiO_2–MCM-48 causes a further decrease of XRD peak intensities (see Fig. 2a). As nitrogen physisorption shows a high porosity for this sample as well (see below), this can be also attributed to the loss of scattering contrast between pores and the walls of the MCM-48 pore system.

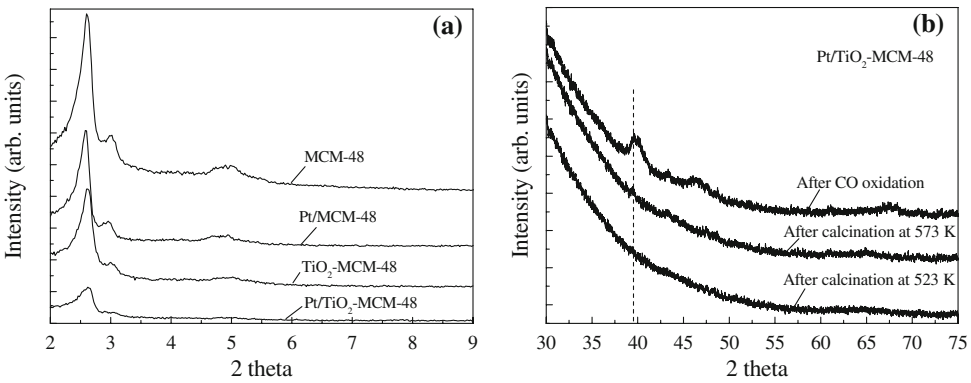

Fig. 2 XRD patterns of MCM-48 with guest species. **a** Low-angle patterns of pure MCM-48, Pt/MCM-48, and Pt/TiO_2–MCM-48. **b** Wide-angle patterns of Pt/TiO_2–MCM-48 after different calcinations and after use in catalysis (cf. Fig. 7)

Figure 2b displays wide-angle XRD patterns for Pt/TiO_2–MCM-48 after various pretreatments, which were collected using a powder diffractometer with position-sensitive detector and 48–72-h exposure times, aiming to detect minor signals of crystalline TiO_2 and Pt. The choice of calcination conditions was guided by preliminary DTA/TG experiments with the Pt precursor employed in the synthesis ($(NH_4)_2PtCl_4$), according to which the reductive precursor decomposition was finished around 573 K (see also below, catalytic results). Hence, whereas the absence of Pt metal reflections was to be expected at a calcination temperature of 523 K, there was almost no Pt signal after precursor decomposition at 573 K as well. This suggests a very high Pt dispersion, apparently favored by the confinement effect of the MCM-48 mesopores. Figure 2b also shows the wide-angle diffractogram of a sample used in catalysis (cf. Fig. 7) which indicated substantial sintering of at least part of the Pt particles.

In Fig. 3a, a typical TEM micrograph of the Pt/TiO_2–MCM-48 composite material is presented. The micrograph shows that single particles often do not scatter coherently. In the image, the upper parts of a mesoporous particle are well aligned with respect to the electron beam and shows the periodicity of the silica MCM-48 framework, whereas the particles shown in the lower part are not in well-aligned position and scattering condition and seem to be amorphous. Slight changes in particle alignment, however, lead to regular and periodic contrast variations and show that these parts are periodically ordered as well. The TEM image, thus, shows the typical lattice fringes of a well-ordered silica MCM-48 host structure with no obvious damage in the periodic structure. Based on this result, it can

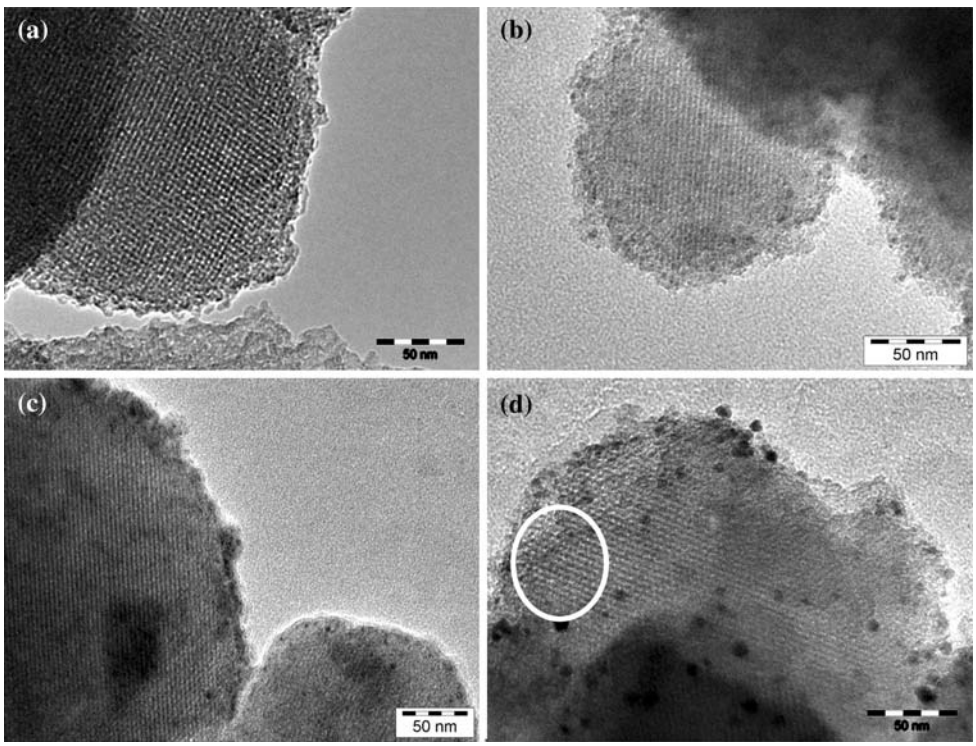

Fig. 3 TEM micrographs of Pt/TiO_2–MCM-48: **a** as-prepared sample, **b** after calcination at 523 K, **c** after calcination at 573 K, and **d** sample after use in catalysis (cf. Fig. 7)

be concluded that after both-impregnation procedures (TiO_2 and Pt), the framework of silica MCM-48 was well maintained. In addition to the confirmation of the integrity of the porous MCM-48, Pt-containing aggregates have been scanned for, but none has been detected on the external MCM-48 surfaces in several TEM micrographs analyzed. Hence, the Pt is well dispersed over the porous matrix. The well-dispersed Pt retains without much agglomeration in the mesopores of TiO_2–MCM-48 even after calcination treatment at 523 K (Fig. 3b); however, at higher calcination temperature of 573 K (Fig. 3c), Pt starts to agglomerate resulting into the particle size of 2 nm, in agreement with XRD results (vide supra). The agglomeration of Pt is more severe for the Pt/TiO_2–MCM-48 sample used in the catalytic experiment (cf. Fig. 7) in the micrograph shown in Fig. 3d, and Pt particles of up to 10-nm size can be seen to be distributed over the external surface of the (intact) MCM-48 particle. However, Pt clusters having survived the catalytic experiment inside the pores can also be discerned (see, e.g., encircled region). In addition, Pt particles can be found near the pore entrances, but still in a size compatible with the pores, maybe as an intermediate stage of the sintering.

Nitrogen adsorption–desorption isotherms and pore-size distribution analysis for parent MCM-48, and the composites made are presented in Fig. 4, and the numerical parameters are listed in Table 1. All the isotherms presented in Fig. 4 are of type IV characteristic of mesoporous materials. The shape of the adsorption isotherm gradually changes from calcined MCM-48 to Pt-incorporated TiO_2–MCM-48, due to impregnation of both titania and platinum inside the mesopores of siliceous MCM-48. From pure MCM-48 to Pt containing TiO_2–MCM-48, the BET surface area decreases from 1194 to 1008 m^2/g, but surprisingly, Pt/MCM-48 is even slightly below. The mesopore volume decreases from 0.87 to 0.68 cm^3/g, this time with Pt/MCM-48 in between. This decrease of BET surface area and pore volume is slightly larger than would be expected (less than 1%) given the low amounts of TiO_2 and Pt introduced. Most likely, a combination of pore blockage and degradation of porosity through sample treatment has taken place. However, the shape of the adsorption isotherms and of the pore-size distributions shows that the structure of the MCM-48 material is preserved in all the functionalized samples, in agreement with XRD and TEM results presented above, and that damage to the pore system is minor contrary to that observed in recent Au/TiO_2–MCM-48 preparations [13].

Figure 5 shows the UV–vis diffuse reflectance spectra of both TiO_2–MCM-48 and Pt/TiO_2–MCM-48 composites together with the reference compound TiO_2 (Rutile). The absence of a broad absorption band at ~325 nm in both Ti-containing mesoporous materials confirms the absence of large TiO_2 particles in the pores and/or outside the pores of MCM-48 matrix. The UV–vis spectra of both composites are also compared with pure rutile-TiO_2. The absorption edge of the TiO_2–MCM-48 sample is observed to be at a shorter wavelength ($\Delta\lambda \sim 30$ nm) than that of the bulk rutile-TiO_2 sample (as shown in Fig. 5), in good agreement with our previous results [11]. This is an indication of a particle-size effect on the absorption energy: the smaller the particle, the shorter is the wavelength. Considering the

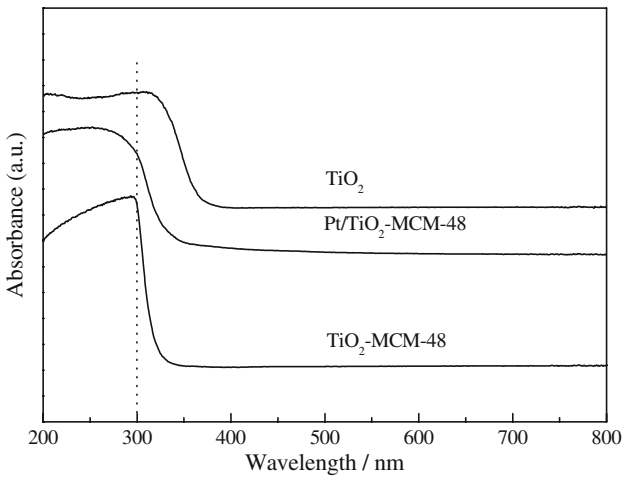

Fig. 5 UV–vis spectra of TiO_2–MCM-48, Pt/TiO_2–MCM-48, and pure rutile TiO_2

Fig. 4 Comparison of nitrogen-adsorption isotherms for impregnated TiO_2–MCM-48, Pt/MCM-48, and Pt/TiO_2–MCM-48. The isotherm for pure MCM-48 from the same batch is also included to facilitate the comparison

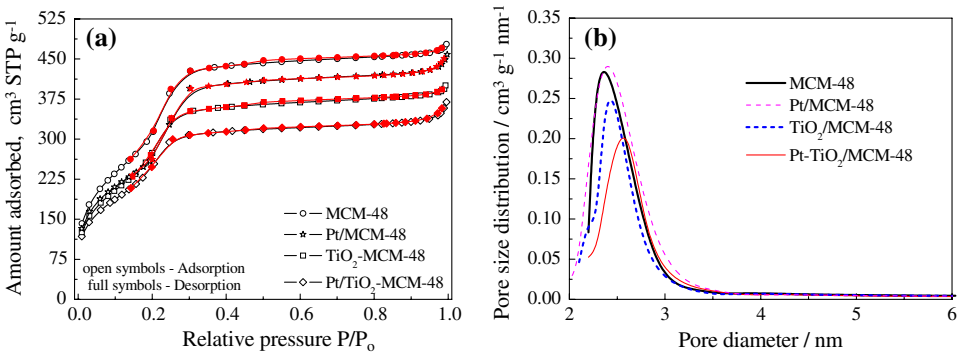

energy shift of approximately 1700 cm^{-1} and using the formalism proposed by Kormann et al. [17], a particle size ~2 nm in diameter is deduced, indicating that the pore channels of MCM-48 provide a size confinement for TiO_2 particles with a maximum size of ~3 nm. After the impregnation of Pt in the TiO_2–MCM-48 support materials, the UV–vis shows the broad maxima at around 265 nm. The blue shift is ascribed to the interaction between titania crystallites and the platinum introduced.

X-ray photoelectron spectroscopy (XPS) has been employed to get more insight into the incorporation of metal/metal oxide into the pore system of MCM-48 and to investigate the nature of the Pt-species on and/or near the external surface of the mesoporous matrix. The XPS results obtained from Pt/TiO_2–MCM-48 in the as-prepared state and after reduction and re-oxidation are presented in Fig. 6 and Table 2. In order to facilitate the comparison of binding energies, an XPS spectrum measured with a Pt foil (as a reference) has also been included. All the samples clearly show two peaks of Pt $4f_{7/2}$ and Pt $4f_{5/2}$ separated by ca. 3.3 eV in agreement with the literature [18].

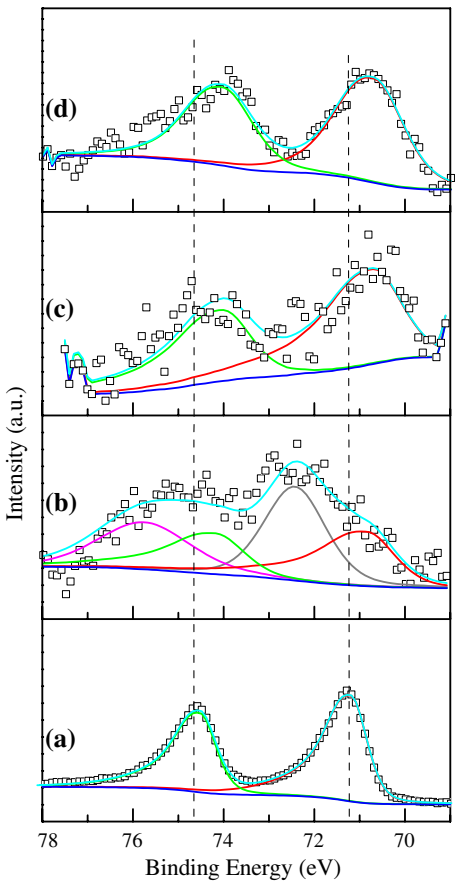

Fig. 6 XPS spectra of Pt 4f region for **a** Pt foil as a reference, **b** as-prepared Pt/TiO_2–MCM-48, **c** reduced Pt/TiO_2–MCM-48, and **d** re-oxidized Pt/TiO_2–MCM-48

Table 2 XPS binding energies and surface atomic ratios of Pt/TiO_2–MCM-48

Sample	BE Pt $4f_{7/2}$ (eV)	Pt/Si atomic ratios	
		XPS	ICP-AES
As-prepared	70.9	0.0056	0.0226
	72.4		
H_2-reduced at 723	70.6	0.0075	0.0226
Re-oxidized at 723 K	70.8	0.0097	0.0226
Pt foil (reference)	71.2	–	–

For as-prepared Pt/TiO_2–MCM-48 sample, the Pt $4f_{7/2}$ emission shows a rather broad line shape which indicates the coexistence of two different oxidation states (Fig. 6). According to our analysis, this sample contained already reduced Pt, with a binding energy of 70.9 eV. The other doublet has a binding energy corresponding to that of the diammonium tetrachloroplatinate(II) precursor used in the synthesis (72.4 eV [19]). It should be noted that the analysis shown in Fig. 6b is not the only possible fit of this rather noisy spectrum, but the conclusion that the as-prepared Pt/TiO_2–MCM-48 sample contained already some reduced Pt will find support in observations made in the catalytic experiments (see below). After reduction of this sample in hydrogen (Fig. 6c), a single Pt 4f doublet was found, with $4f_{7/2}$ at 70.6 eV, i.e., clearly below the binding energy measured with the bulk Pt foil. Further oxidation treatment to the reduction-pretreated sample in flowing O_2/Ar gas mixture at 723 K did not lead to partial/full oxidation of metallic platinum as it is apparent from the Pt $4f_{7/2}$ emission observed at 70.8 eV. However, the line asymmetry typical for Pt was significantly suppressed.

The negative binding energy shifts of Pt relative to the bulk Pt foil (cf. Table 2) seem to be characteristic for the Pt/TiO_2–MCM-48 composite. Similar negative binding energy shifts have been recently found in the Au/TiO_2–MCM-48 system [13], and earlier on in studies with Ru/Al_2O_3 and Ru/TiO_2 catalysts where two different binding energies for supported metal species and strong differences in line asymmetry were found as well [20]. Although an unanimous discussion of XPS binding energies is difficult due to the various possible origins of binding-energy shifts, the results may well indicate an interaction of the metallic platinum with the TiO_2 component in the matrix, although it cannot be inferred that a classical Strong Metal–Support Interaction (SMSI) effect [14] has occurred. From Table 2, it can also be seen that the Pt/Si atomic ratios in the surface region are lower than the bulk atomic ratios, which indicates that there is no enrichment of platinum in the external surface region. Thus, the XPS data give evidence that the platinum is well dispersed inside the mesopores of TiO_2–MCM-48.

Table 3 H_2-chemisorption data for Pt encaged in TiO_2–MCM-48 and in MCM-48

Treatment	H_2 chemisorption capacity (μmol g^{-1})	Metal dispersion[a] (%)	Average crystallite size[b] (nm)
Pt/TiO_2–MCM-48			
Red. H_2; 573 K	3.8	14.8	7.7
Red. H_2; 773 K	1.2	4.7	24
ReOx. O_2; 773 K + Red. H_2; 573 K	0.6	2.4	48
Pt/MCM-48			
Red. H_2; 573 K	8.3	18.5	6.1
Red. H_2; 773 K	3.1	6.9	16

[a] Ratio of exposed to present Pt atoms, assumed chemisorption stoichiometry—Pt:1 = 1

[b] According to $d = 6p/(\rho_{pt}A_mN_m)$, with p platinum wt%, ρ_{pt} platinum density, A_m area per H atom, N_m chemsorption capacity, assumptions: spherical particle with full exposure to gas phase, H/Pt = 1

H_2-chemisorption data measured with Pt/TiO_2–MCM-48 after different pretreatments are listed in Table 3 and compared with data from Pt/MCM-48. After reduction in H_2 at 573 K, a chemisorption capacity of 3.8 μmol g^{-1} was obtained, which indicates that ≈15% of the Pt atoms are exposed to the gas phase. Assuming spherical particle shape, this can be transformed into a particle size of almost 8 nm, i.e., clearly larger than the pore diameter. However, in this calculation, full exposure of the particle surface is tacitly assumed, which is unrealistic for the present case. In a mesopore system, the particle surface may be substantially shielded from the gas phase by the matrix walls when the particle size approaches the pore size. Hence, our data do not necessarily indicate growth of the particle beyond the pore size. The chemisorption capacity of Pt/MCM-48 was larger only due to the higher Pt content, and the metal dispersion was indeed very similar. Catalyst reduction was also performed at 773 K to check whether the typical SMSI behavior (shielding of Pt by TiO_{1-x} migrating onto it) occurred in our system. Indeed, this treatment caused the hydrogen chemisorption capacity of Pt/TiO_2–MCM-48 to decrease strongly. However, SMSI has to be reversible upon reoxidation of the catalyst [21, 22], and the data of the third entry in Table 3 show that this was not the case. Apparently, our treatments caused only sintering of the Pt particles. The parallel measurement with Pt/MCM-48 confirmed that Pt particles on this kind of support are not stable upon reduction at 773 K.

The results of the catalytic tests are reported in Figs. 7 and 8. In Fig. 7, the CO conversion curves of four subsequent runs with the same catalyst are shown. Pt/TiO_2–MCM-48 is indeed active for CO oxidation though being

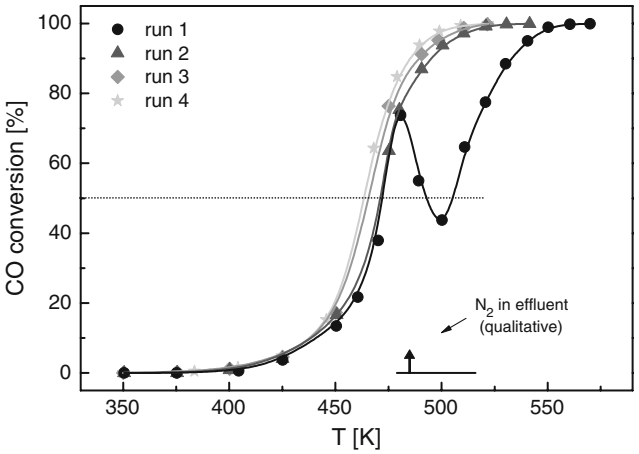

Fig. 7 CO conversions for consecutive runs during CO-oxidation over Pt/TiO_2–MCM-48. The temperature range of N_2 evolution during the first run is indicated, the upright arrow marking the maximum evolution rate

clearly short of the analogous Au/TiO_2–MCM-48 system [13]. The light-off temperatures (temperatures of 50% conversion) even decreased slightly in subsequent runs, from 473 to 461 K. Remarkably, the conversion curve in run 1 is very close to those of the following runs although the Pt precursor was not reduced prior to the experiment. Around 485 K, CO conversion dropped significantly and recovered only at ≈20 K higher temperatures. In this deactivation region, nitrogen was detected in the effluent by the QMS as indicated in the figure. This is rather a clear indication for platinum reduction by the ammonia nitrogen. As it is highly unlikely that an oxidized Pt phase should have a CO oxidation activity comparable to that of Pt metal, the high initial activity of the Pt sample supports the observation from XPS that Pt/TiO_2–MCM-48 contains some metallic Pt already after the impregnation and drying steps of the preparation. A similar observation has been recently made with Au/TiO_2–MCM-48 [13]. Above 480 K, the $(NH_4)_2PtCl_4$ also present was apparently decomposed, which set free nitrogen, but at the same time would make available chloride, which is a catalyst poison to platinum. The rough coincidence between the maximum of the N_2 signal and minimum in the CO conversion curve indeed supports this view which, however, needs to be substantiated in ongoing research.

A similar behavior was observed for the TiO_2-free sample, but there are remarkable differences. Figure 8 shows the conversion curves of four subsequent runs with the Pt/MCM-48 catalyst, and the first and fourth run with Pt/TiO_2–MCM-48 are indicated for comparison. In Pt/MCM-48, precursor reduction took place at significantly higher temperatures (around 515 K). It was then faster than in the TiO_2-containing sample, and the transient poisoning effect was much more intense. As opposed to the latter,

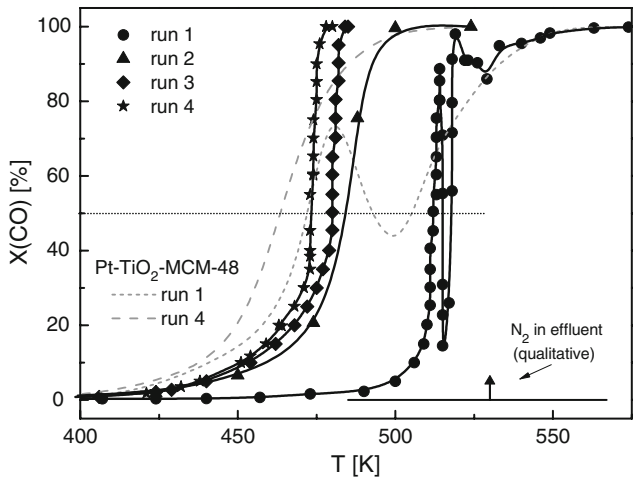

Fig. 8 CO conversions for consecutive runs during CO-oxidation over Pt/MCM-48 (first and fourth run of Pt/TiO_2–MCM-48 given for comparison). The temperature range of N_2 evolution during the first run is indicated, the upright arrow marking the maximum evolution rate

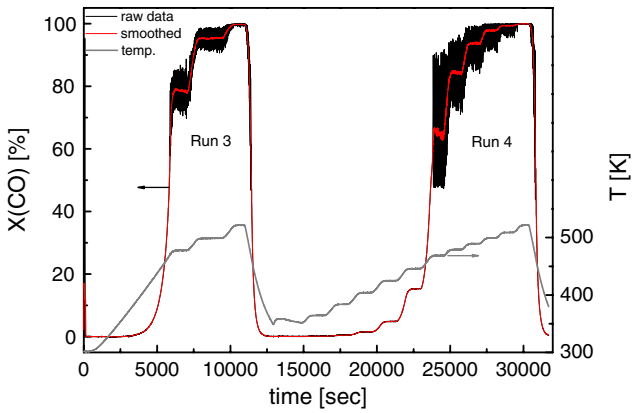

Fig. 9 CO conversions and temperature versus run time for the third and fourth CO oxidation run with Pt/TiO_2–MCM-48 (cf. Fig. 7). The oscillatory behavior is obvious, with its intensity increasing in consecutive runs. The arrows indicate the conversions at which the oscillation commenced

Pt/MCM-48 gave almost no CO conversion below the reduction temperature. After the second run, the light-off temperature was stabilized around 475 K, which is somewhat higher than with Pt/TiO_2–MCM-48 despite the higher Pt content. From the third run on, the catalyst exhibited a pronounced ignition behavior, which was not seen with Pt/TiO_2–MCM-48.

The CO conversion curves in Fig. 7 are partly composed of averaged data, because the CO conversion exhibited pronounced stable oscillations in certain temperature ranges. This is exemplified in Fig. 9 where CO conversions and related temperatures (right-hand axis) of two runs are re-plotted over the time-on-stream. At ca. 470 K, the actual CO conversions begin to oscillate around an average value, which is given in red while the excursions are indicated in black. The oscillations commenced at slightly different temperatures and, hence, different conversions in different runs (in Fig. 9, run 3: $T_{start} = 478$ K, $X \approx 70\%$, run 4: $T_{start} = 468$ K, $X \approx 58\%$) except for the first one where they were completely absent. Catalytic oscillations can be caused by non-linear kinetics of the surface reaction, but also by coupling of surface kinetics with mass and/or heat transfer [23]. Their detailed study is beyond the scope of our investigation. The changes in the conditions under which the oscillations were first observed may be related to the slight increase of oxidation activity in subsequent runs. With Pt/MCM-48, oscillations were not observed under any reaction conditions.

It should be noted that the catalytic data provide serious indications for Pt-TiO_2 interactions on our Pt/TiO_2–MCM-48 catalyst. As opposed to the Au/TiO_2–MCM-48 system where Au could not be deposited in a TiO_2-free MCM-48 matrix by the route employed [13], the deposition of Pt on SiO_2 is straightforward and was successful here as well. Therefore, interaction between Pt and TiO_2 needs to be proven independently. Whereas the related data in our characterization studies (UV blue shift, XPS binding energies) are ambiguous, the catalytic data suggest at least a proximity between TiO_2 aggregates and Pt particles. We infer this not so much from the CO conversions of the reduced catalysts (runs 2–4), which are influenced by a number of unknown quantities (Pt particle-size distribution and segregation, heat and mass transfer phenomena), but merely from the initiation of the reaction by precursor decomposition. Indeed, the significant difference in precursor decomposition (cf. run 1 in Figs. 7 and 8, temperature ranges of N_2 evolution reported graphically in the panels), and the very different course of the CO conversion below this temperature suggesting some "premature" Pt reduction. This can be plausibly explained only by interactions of the $(NH_4)_2PtCl_4$ precursor with the TiO_2 component during impregnation and/or drying. Therefore, one may expect Pt particles (not necessarily all of them!) in the vicinity of TiO_2 aggregates after reduction as well.

The failure to observe the typical SMSI behavior in our chemisorption experiments is, however, at variance with this hypothesis. We believe that this is due to the low TiO_2 content in our samples, maybe combined with an influence of the SiO_2 matrix on the highly disperse TiO_2 entities. Further study with preparations containing more TiO_2 is now under way to solve this problem.

Conclusions

In conclusion, it has been demonstrated that it is possible to introduce highly dispersed platinum nanoparticles in the

pores of TiO_2–MCM-48 using a conventional wetness-impregnation method. XRD, TEM, N_2-physisorption measurements confirm the deposition of the platinum precursor inside the pores of the mesoporous matrix without destroying their integrity. XPS indicates the presence of metallic platinum already in the unreduced Pt/TiO_2–MCM-48, which coexists with the unaffected precursor. Upon mild reduction (reductive thermal decomposition), highly disperse Pt particles were formed. The platinum tends, however, to sintering and segregation upon reduction in hydrogen at higher temperatures or during use in CO oxidation. Remarkable differences in CO oxidation activity of unreduced Pt/TiO_2–MCM-48 and Pt/MCM-48 catalysts suggest that synergetic interaction between the precursor and TiO_2–MCM-48 system makes the former catalyst better than the latter, due to proximity between Pt and titania clusters.

Acknowledgements We acknowledge financial support provided by the Deutsche Forschungsgemeinschaft in the frame of the Sonderforschungsbereich ''Metal-substrate interactions in heterogeneous catalysis'', SFB 558 (Projects B3 and A3). The authors are grateful to Ms. S. Buse for her help during chemisorption measurements.

References

1. Beck JS, Vartuli JC, Roth WJ, Leonowicz ME, Kresge CT, Schmitt KD, Higgins JL, Schlenker JL (1992) J Am Chem Soc 114:10834
2. Kresge CT, Leonowicz ME, Roth WJ, Vartuli JC, Beck JS (1992) Nature 359:710
3. Sayari A (1996) Chem Mater 8:1840
4. Corma A (1997) Chem Rev 97:2373
5. Hoppe R, Ortlam A, Rathousky J, Schulz-Ekloff G, Zukal A (1997) Microporous Mater 8:267
6. Kinski I, Gies H, Marlow F (1997) Zeolites 19:375
7. Schulz-Ekloff G, Wöhrle D, van Duffel B, Schoonheydt RA (2002) Microporous Mesoporous Mater 51:91
8. On DT, Desplantier-Giscard D, Danumah C, Kaliaguine S (2001) Appl Catal A 222:299
9. Gies H, Grabowski S, Bandyopadhyay M, Grünert W, Tkachenko OP, Klementiev KV, Birkner A (2003) Microporous Mesopor Mater 60:31
10. van den Berg MWE, Polarz S, Tkachenko OP, Klementiev KV, Bandyopadhyay M, Khodeir L, Gies H, Muhler M, Grünert W (2006) J Catal 241:446
11. Bandyopadhyay M, Birkner A, van den Berg MWE, Klementiev KV, Schmidt W, Grünert W, Gies H (2005) Chem Mater 17:3820
12. Bandyopadhyay M, Korsak O, van den Berg MWE, Grünert W, Birkner A, Li W, Schüth F, Gies H (2006) Microporous Mesopor Mater 89:158
13. Narkhede VS, Toni AD, Narkhede VV, Guraya M, Niemantsverdriet JW, van den Berg MWE, Grünert W, Gies H (2009) Microporous Mesopor Mater 118:52
14. Tauster SJ, Fung SC, Garten RL (1978) J Am Chem Soc 100:170
15. Chatterjee M, Iwasaki T, Onadera Y, Nagase T (1999) Catal Lett 61:199
16. Jang JH, Lee SC, Kim DJ, Kang M, Choung SJ (2005) Appl Catal A 286:36
17. Kormann C, Bahnemann DW, Hoffmann MR (1988) J Phys Chem 92:5196
18. Moulder LF, Stickle WF, Sobol PE, Bomben KD (1992) Handbook of X-ray photoelectron spectroscopy. Perkin-Elmer Cooperation, USA
19. Katrib A, El-Egaby MS (1979) Inorg Chim Acta 36:L405
20. Elmasides C, Kontarides DI, Grünert W, Verykios XE (1999) J Phys Chem B 103:5227
21. Uchijima T (1996) Catal Today 28:105
22. Grünert W, Brückner A, Hofmeister H, Claus P (2004) J Phys Chem B 108:5709
23. Slinko MM, Jäger NI (1994) Stud Surf Sci Catal 86:1